Contrasting responses to increasing dissolved iron on photosynthesis and O$_2$ availability in the gastric cavity of two Mediterranean corals.

Walter Dellisanti [Corresp., 1], **Qingfeng Zhang** [1], **Christine Ferrier-Pagès** [2], **Michael Kühl** [1]

[1] Department of Biology, Marine Biology Section, University of Copenhagen, Helsingør, Denmark

[2] Coral Ecophysiology Laboratory, Center Scientifique de Monaco, Principality of Monaco, Monaco

Corresponding Author: Walter Dellisanti
Email address: walter.dellisanti@gmail.com

Iron (Fe) plays a fundamental role in coral symbiosis, supporting photosynthesis, respiration, and many important enzymatic reactions. However, the extent to which corals are limited by Fe and their metabolic responses to inorganic Fe enrichment remains to be understood. We used respirometry, variable chlorophyll fluorescence, and O$_2$ microsensors to investigate the impact of increasing Fe(III) concentrations (20, 50, and 100 nM) on the photosynthetic capacity of two Mediterranean coral species, *Cladocora caespitosa* and *Oculina patagonica*. While the bioavailability of inorganic Fe can rapidly decrease, we nevertheless observed significant physiological effects at all Fe concentrations . In *C. caespitosa*, exposure to 50 nM Fe(III) increased rates of respiration and photosynthesis, while the relative electron transport rate (rETR(II)) decreased at higher Fe(III) exposure (100 nM). In contrast, *O. patagonica* reduced respiration, photosynthesis rates, and maximum PSII quantum yield (F$_v$/F$_m$) across all iron enrichments. Both corals exhibited increased hypoxia (< 50 μmol O$_2$ L^{-1}) within their gastric cavity at night when exposed to 50 and 100 nM Fe(III), leading to increased polyp contraction time and reduced O$_2$ exchange with the surrounding water. Our results indicate that *C. caespitosa*, but not *O. patagonica*, might be limited in Fe for achieving maximal photosynthetic efficiency. Understanding the multifaceted role of iron in corals' health and their response to environmental change is crucial for effective coral conservation.

Contrasting responses to increasing dissolved iron on photosynthesis and O_2 availability in the gastric cavity of two Mediterranean corals.

Walter Dellisanti[1], Qingfeng Zhang[1], Christine Ferrier-Pagés[2], Michael Kühl[1]

[1] Marine Biology Section, Department of Biology, University of Copenhagen,
Strandpromenaden 5, 3000, Helsingør, Denmark.
[2] Coral Ecophysiology Laboratory, Centre Scientifique de Monaco, Quai Antoine 1er 8, 98000,
Monaco, Principality of Monaco.

Corresponding Author:
Walter Dellisanti[1]
Strandpromenaden 5, 3000, Helsingør, Denmark
Email address: walter.dellisanti@bio.ku.dk

Abstract

Iron (Fe) plays a fundamental role in coral symbiosis, supporting photosynthesis, respiration, and many important enzymatic reactions. However, the extent to which corals are limited by Fe and their metabolic responses to inorganic Fe enrichment remains to be understood. We used respirometry, variable chlorophyll fluorescence, and O_2 microsensors to investigate the impact of increasing Fe(III) concentrations (20, 50, and 100 nM) on the photosynthetic capacity of two Mediterranean coral species, *Cladocora caespitosa* and *Oculina patagonica*. While the bioavailability of inorganic Fe can rapidly decrease, we nevertheless observed significant physiological effects at all Fe concentrations. In *C. caespitosa*, exposure to 50 nM Fe(III) increased rates of respiration and photosynthesis, while the relative electron transport rate (rETR(II)) decreased at higher Fe(III) exposure (100 nM). In contrast, *O. patagonica* reduced respiration, photosynthesis rates, and maximum PSII quantum yield (F_v/F_m) across all iron enrichments. Both corals exhibited increased hypoxia (< 50 μmol O_2 L^{-1}) within their gastric cavity at night when exposed to 50 and 100 nM Fe(III), leading to increased polyp contraction time and reduced O_2 exchange with the surrounding water. Our results indicate that *C. caespitosa*, but not *O. patagonica*, might be limited in Fe for achieving maximal photosynthetic efficiency. Understanding the multifaceted role of iron in corals' health and their response to environmental change is crucial for effective coral conservation.

Introduction

Scleractinian corals are the foundation species of tropical coral reefs and temperate coralligenous assemblages (Hoeksema, 2017; Ingrosso et al., 2018). Their metabolic processes (i.e., cellular

40 respiration, symbiont photosynthesis, calcification), as well as cellular homeostasis (Reich et al.,
41 2023), are linked to macro- and micro-nutrient availability through host feeding and nutrient
42 uptake by endosymbionts (Muscatine & Porter, 1977; Houlbrèque & Ferrier-Pagès, 2009; Houk
43 et al., 2020). Among micro-nutrients, iron is fundamental for cellular function and metabolism
44 (Raven, Evans & Korb, 1999; Behrenfeld & Milligan, 2013; D'Angelo & Wiedenmann, 2014;
45 Reich et al., 2020). However, the impacts of iron on coral metabolism are multifaceted.
46 Iron exists in seawater in two oxidation states, Fe(II) and Fe(III), and can be found as "free" ions
47 or complexed with organic and inorganic ligands (Liu & Millero, 2002; Blain & Tagliabue,
48 2016). The availability of iron in aerated seawater is primarily as Fe(III), due to the
49 complexation of Fe(II) by strong iron-binding ligands (Johnson, Gordon & Coale, 1997), such as
50 inorganic oxides, extracellular polymeric exudates from phytoplankton, or siderophores
51 produced by bacteria (Walte & Morel, 1984; Gledhill et al., 2004; Hassler et al., 2011).
52 Dissolved iron is mostly adsorbed by photosynthetic symbionts and supports the photosynthetic
53 process in corals via its role as a cofactor in proteins involved in photosynthesis, electron
54 transport, and scavenging enzymes for reactive oxygen species (Raven, Evans & Korb, 1999;
55 Reichelt-Brushett & McOrist, 2003; Reich et al., 2020). Iron deficiency can thus significantly
56 limit coral photosynthesis, potentially resulting in reduced growth rates, compromised skeletal
57 development, and impaired energy acquisition (Entsch, Sim & Hatcher, 1983; Ferrier-Pagès et
58 al., 2001; Shick et al., 2011). However, exposure to high metal concentrations, including iron,
59 can also disrupt the coral symbiosis and lead to bleaching (Harland & Brown, 1989; Reichelt-
60 Brushett & McOrist, 2003; Leigh-Smith, Reichelt-Brushett & Rose, 2018). The availability of
61 inorganic iron also influences the biogeochemical cycling of other trace metals (Rodriguez et al.,
62 2016), acting as essential cofactors in numerous enzymatic and biochemical reactions (Morrissey
63 et al., 2015; Sutak, Camadro & Lesuisse, 2020). Therefore, a disruption in trace metal dynamics
64 may further exacerbate the physiological stress experienced by corals due to combined
65 environmental changes (i.e., rising temperatures, ocean acidification, nutrient pollution) (Ponti et
66 al., 2021), leading to oxidative stress (Leigh-Smith, Reichelt-Brushett & Rose, 2018).This can
67 ultimately impact the capacity of corals to withstand environmental changes, leading to
68 decreased resilience and survival.
69 Key metabolic activities in corals occur in their gastric cavity (coelenteron), which plays an
70 important role in processes like digestion, excretion, and internal nutrient cycling but remains
71 largely unexplored (Hughes et al., 2022). Due to the presence of photosynthetic endosymbionts
72 living in symbiosis within the coral endoderm facing the coelenteron, O_2 levels within the gastric
73 cavity are strongly influenced by light conditions and can vary with depth. In the upper region of
74 the gastric cavity, the O_2 levels can be as high as 400% air saturation (Agostini et al., 2012),
75 while deeper regions of the gastric cavity can exhibit lower O_2 levels reaching hypoxia or even
76 anoxia (Agostini et al., 2012), especially in darkness. Such O_2 dynamics influence the types of
77 microorganisms that thrive within the gastric cavity (Agostini et al., 2012; La Rivière, Garel &
78 Bally, 2016) and might also affect trace metal and nutrient availability via O_2-dependent redox
79 changes in the gastric cavity. There is thus a need for further research to explore the role of trace

80 metals, specifically dissolved iron, within the gastric cavity and to examine how iron enrichment
81 might impact the availability of O_2 in this critical microenvironment.
82 While the effects of metals on coral physiology, have been studied in tropical corals (Ferrier-
83 Pagès et al., 2001; Reichelt-Brushett & McOrist, 2003; Reich et al., 2023), this is not the case for
84 temperate corals. These corals are often more exposed to anthropogenic activities, which
85 increase metal levels in seawater and sediments (Mahowald et al., 2005; Krishnamurthy et al.,
86 2010). For example, Mediterranean corals are the key species of the Marine Animal forests
87 (MAFs), which exhibit a high biodiversity of marine species and provide important ecosystem
88 services and functions (Fine, Zibrowius & Loya, 2001; Kružić & Benković, 2008; Ingrosso et al.,
89 2018; Bevilacqua et al., 2021). These forests receive diverse inputs of inorganic iron from both
90 natural and anthropogenic sources, including atmospheric deposition, terrestrial runoff, and
91 hydrothermal vents (Sarthou & Jeandel, 2001; Bonnet & Guieu, 2006; Molari et al., 2018). Such
92 diverse sources contribute to spatial and temporal heterogeneity in iron concentrations and thus
93 the availability of this trace metal to marine organisms (Guerzoni et al., 1999; Wagener, Guieu &
94 Leblond, 2010; Gallisai et al., 2014). Iron levels in Mediterranean seawater typically vary from
95 0.7 to 14.5 nM in coastal regions (Sarthou & Jeandel, 2001), and iron enrichment has been found
96 prevalent in coastal sediments near harbors in the Gulf of Genoa and the Adriatic Sea (Bertolotto
97 et al., 2005; Orlov et al. 2021).. In comparison, these iron levels are generally higher than those
98 recorded in Caribbean and Indo-Pacific waters (<5 nM, GEOTRACES IDP, 2021). Within the
99 Mediterranean Sea, *C. caespitosa* and *O. patagonica* are two key coral species serving as
100 bioindicators for water quality in the Mediterranean Sea (Fine, Zibrowius & Loya, 2001; Peirano
101 et al., 2004; Rodolfo-Metalpa et al., 2006; Kružić & Benković, 2008; Casado de Amezua et al.,
102 2015) and they are naturally exposed to varying levels of inorganic trace metals. However, the
103 role and effect of dissolved iron in these symbiont-bearing corals remains unknown.
104 In this study, we explore the effect of increasing Fe(III) levels on respiration and photosynthesis,
105 as well as on the internal O_2 status of the gastric cavity, in two common Mediterranean corals,
106 *Cladocora caespitosa* and *Oculina patagonica*. We hypothesized that low to moderate Fe(III)
107 exposure may support their photosynthetic capacity and physiological status, while excessive
108 amounts of Fe(III) above a certain threshold have detrimental effects on coral physiology. Our
109 results indicate that a short-term enrichment of dissolved iron might be beneficial in the host-
110 symbiont relationship of corals living in an iron-limited environment, providing new insights
111 into the metabolic responses of corals to trace metals.
112

Materials & Methods

114 Three healthy colonies (20 to 30 cm²) of *Cladocora caespitosa* were collected from Trieste
115 (Italy, 45.707° N, 13.712° E) using SCUBA in April 2023 (CITES IT/EX/2023/MCE/00335).
116 Subsequently, the corals were carefully placed in a container with aerated seawater (50 L) and
117 transported to the laboratory in Monaco. Ten colonies of *Oculina patagonica* (10 to 20 cm²)
118 were originally sampled in Albissola, Gulf of Genoa(Italy, 44.283° N, 8.50° E) as previously
119 described (Rodolfo-Metalpa et al., 2006) and were kept in flow-through aquaria in Monaco that

120 were continuously supplied with non-filtered seawater sampled from ~50 meters depth and
121 heated to 18°C. Three colonies of *O. patagonica* were randomly selected and used in this study.
122 Corals were exposed to a 12:12 h light-dark cycle under a photon irradiance (400-700 nm) of 150
123 ± 10 µmol photons m^{-2} s^{-1} provided by 400 W metal halide lamps (HQI-TS, Philips). The coral
124 colonies were fragmented into 48 nubbins (n = 24 per species) and placed on PVC support using
125 epoxy resin putty. The nubbins of *C. caespitosa* consisted of single polyps ~2 cm^2, and those of
126 *O. patagonica* consisted of multiple polyps with an approximate size of ~5 cm^2 (Fig. 1). Corals
127 were fed twice a week with *Artemia salina* nauplii and were allowed to acclimate to the
128 aquarium conditions for two weeks before the onset of experiments.
129 The experimental design consisted of four 8 L tanks; one tank was maintained without Fe(III)
130 addition, while the other tanks were used for the iron enrichment experiments. The tanks were
131 filled with the same non-filtered seawater and maintained under controlled conditions in a water
132 bath at 18°C with a photoperiod of 12:12 and an incident photon irradiance (400-700 nm) of 150
133 ± 10 µmol photons m^{-2} s^{-1}, as measured with a Universal Light Meter (ULM-500) equipped with
134 a spherical micro quantum sensor (US-SQS/L, Heinz Walz, Effeltrich, Germany). Following two
135 weeks of acclimation, the nubbins (n = 6 per species per condition) were randomly mixed and
136 transferred into the tanks where they were kept unfed.
137 A stock solution of Fe(III) (50 µM $FeCl_3*6H_2O$, Sigma-Aldrich) was prepared for the iron
138 enrichment experiments. Two pulses of Fe(III) were added per day by diluting the stock solution
139 to expose corals to 0, 20, 50, and 100 nM Fe / day, hereafter named "control", "20Fe", "50Fe",
140 and "100Fe", and the experiment lasted one week. No water renewal was carried out during the
141 experimental period. After one week of exposure, seawater samples (15 mL) were collected in
142 metal-free tubes (Labcon) from the tanks for elemental iron determination and from the
143 respirometry chambers for measuring iron uptake (see below). The final iron concentration was
144 measured in 0.32 M HNO_3 diluted samples using inductively coupled plasma mass spectrometry
145 (ICP-MS, iCAP-Q, Thermo Scientific). The uptake rate was calculated as the absolute difference
146 of Fe measured in the chambers from the Fe measured in the tanks and Fe concentration was
147 expressed in µg L^{-1}.
148 The net production/consumption of dissolved oxygen (O_2) due to coral photosynthesis and
149 respiration was measured using custom-made respirometry chambers (55 mL) composed of
150 transparent polycarbonate (Fig. S1). The chambers were closed with a gas-tight transparent lid
151 and contained a magnetic stirrer below a perforated plate at the bottom to ensure water mixing
152 during incubation. An O_2-sensitive optical sensor spot (OXSP5-ADH, Pyroscience GmbH) was
153 attached to each chamber's internal surface and was read out via a fiber optic cable (SPFIB-LNS,
154 Pyroscience GmbH) fixed via a holder on the outside of the transparent chamber wall and
155 connected to a fiber-optic O_2 meter (FSPRO-4, Pyroscience GmbH). The meter was connected
156 via a USB cable to a PC running the data-logging software (Pyro Workbench; Pyroscience
157 GmbH). Prior to experimental measurements, sensors were calibrated in µmol O_2 L^{-1} using a 2-
158 point calibration, measuring the sensor signals in anoxic (seawater with Na_2SO_3) and 100% air-
159 saturated seawater at experimental temperature and salinity.

160   Dissolved oxygen was recorded every second during the incubation of corals. Dark respiration

161   (R) and net photosynthesis (P_n) were calculated from the linear change in O_2 concentration over

162   time measured during 30-min dark and 30-min light incubations, and the rates were calculated as

163   ($\Delta O_2/\Delta t$) x V/A, where V is the volume of seawater surrounding the coral samples in the

164   chamber and A is the coral surface area. The coral surface area was determined with the

165   aluminum foil technique (Marsh, 1970). The surface area of the aluminum foil used to cover

166   living tissue was determined using the ImageJ software v. 1.53 (Schneider, Rasband & Eliceiri,

167   2012).

168   Gross photosynthesis (P_g) was calculated by adding the absolute value of R to P_n, assuming that

169   the dark respiration was identical to respiration in the light. Subsequently, P_g:R ratios were

170   calculated as a measure of the diurnal productivity and degree of autotrophy of the coral

171   holobiont. We note that while P_g can be assigned to the photosynthesis of endosymbionts, R is

172   affected by the respiratory activity of the coral host, its photosynthetic endosymbionts as well as

173   its microbiome.

174   The photosynthetic capacity of the endosymbionts in the coral samples was assessed with

175   variable chlorophyll fluorimetry using a Pulse Amplitude Modulated (PAM) fluorometer (Dual-

176   PAM, Heinz Walz, Effeltrich, Germany) equipped with a standard glass-fiber optic probe (Ralph

177   et al., 1999). These measurements were obtained at the end of each iron enrichment period from

178   single polyp measurements of each coral (n = 5 per condition), after 15 min dark acclimation.

179   The maximum photochemical quantum yield of PSII (F_v/F_m) was calculated as (Schreiber, 2004):

180   $F_v/F_m = (F_m-F_0)/F_m$, where F_m is the maximum fluorescence yield measured during a strong

181   saturation pulse (3000 µmol photon m^{-2} s^{-1}, width 600 ms) and F_0 is the minimum fluorescence

182   yield before the saturation pulse using weak measuring light pulses (<1 µmol photon m^{-2} s^{-1},

183   width 3 µs, frequency 0.6 kHz). The minimum fluorescent yield, F_0, is measured when all PSII

184   centers are open and can be used as a proxy for chlorophyll biomass (Serôdio, Da Silva &

185   Catarino, 1997), while the maximum fluorescence yield, F_m, is measured when all PSII centers

186   are closed in response of the saturation pulse (Baker et al., 2001). Rapid light curves (RLCs)

187   were measured by illuminating dark-adapted corals at increasing irradiance from 0 to 2000 µmol

188   photon m^{-2} s^{-1} (PAR) with 20 s incubation at each irradiance step (Ralph & Gademann, 2005;

189   Trampe et al., 2011). The effective photochemical quantum yield of PS(II) was calculated as

190   $Y(II) = (F'_m-F)/F_m$ (Genty, Briantais & Baker, 1989) and provides a measure of the PSII

191   photosynthetic capacity. The rETR was calculated from Y(II) and the actinic photon irradiance,

192   E_d, as rETR = Y(II) $\times$ E_d and represents a relative measure of the PSII electron transport rate

193   (Beer et al., 1998). All rETR, F_v/F_m, and Y(II) yields were calculated using the system software

194   (WinControl, Heinz Walz GmbH, Germany).

195   Clark-type, electrochemical O_2 microsensors with a slender shaft and a tip diameter of 50 µm

196   (OX-50, Unisense A/S, Denmark) were used to measure the O_2 distribution within the gastric

197   cavity of corals under light exposure and in darkness. Additionally, overnight O_2 fluctuations (6

198   p.m. to 6 a.m.) were continuously recorded in the dark with the microsensor tip positioned in the

199   lower part of the gastric cavity.

200 For microsensor measurements, coral polyps (n = 3) were placed inside a custom-designed flow
201 chamber (0.8 L), with a consistent laminar water flow (0.5 cm s^{-1}) of oxygenated seawater (18°C
202 and salinity of 35) as previously described by Haro et al. (2019). During light incubation, the
203 corals were illuminated with a fiber optic lamp (KL 2500 LED, Schott) with known photon
204 irradiance (400-700 nm) levels of 150 ± 10 μmol photons m^{-2} s^{-1}, as determined by a Universal
205 Light Meter (ULM-500) equipped with a spherical micro quantum sensor (US-SQS/L, Heinz
206 Walz, Effeltrich, Germany). The O_2 microsensors were linearly calibrated from sensor signal
207 readings in 100% air-saturated seawater and anoxic water (using sodium ascorbate solution). The
208 O_2 microsensor was mounted on a motorized micromanipulator system (Unisense A/S,
209 Denmark) and was connected to a microsensor meter (fx-6 UniAmp, Unisense A/S, Denmark).
210 The micromanipulator and microsensor meter were connected to a PC running dedicated
211 software for data acquisition and sensor positioning (SensorSuite Profiler v3.2, Unisense A/S,
212 Denmark). The positioning of the microsensor tip relative to the coral surface was observed via a
213 dissection microscope and a digital USB microscope (Dino-Lite 5MP Edge, AnMo Electronics,
214 Taiwan).
215 For measurements in the gastric cavity, one depth profile was measured per coral polyp.
216 The microsensor tip was initially positioned at the center of the coral mouth, after which was
217 lowered vertically using the micromanipulator by 50-100 μm steps until a contraction of the
218 coral polyp was observed. This position was identified as the base of the gastric cavity. After the
219 microsensor signal was stable (minimum 10 min), depth profiles of O_2 concentration were
220 measured by moving stepwise from the cavity's base toward the mouth and concluding (~2 mm)
221 in the seawater above the coral mouth. For tracking temporal O_2 variations overnight within the
222 gastric cavity under dark conditions, the microsensor remained positioned at the base of the coral
223 gastric cavity. One temporal profile was measured per coral polyp. Concurrently, a digital
224 microscope (Dino-Lite 5MP Edge, AnMo Electronics, Taiwan) was employed to capture time-
225 lapse imagery of coral contractions simultaneously with the O_2 concentration measurements
226 (https://doi.org/10.5281/zenodo.10698045), with frames captured every 2 minutes using
227 DinoCapture 2.0 software. The time-lapse videos were checked for polyp contraction every 3
228 frames (every 6 minutes in real-time), and the contraction was marked by tentacle retraction and
229 reduction in the relative height of the oral disk. The percentage of contraction time was
230 calculated by dividing the number of frames in which contraction occurs by the total number of
231 examined frames.
232 All data were log10-transformed and checked for normality using the Shapiro-Wilk test and for
233 homogeneity of variance using Levene's test. When data did not meet the assumptions of
234 normality, a Kruskal-Wallis test was used with the Wilcoxon rank test for pairwise comparison.
235 Parametric one-way analysis of variance (ANOVA) with the Tukey HSD test was used for data
236 that followed a normal distribution. A linear regression model was used to estimate the oxygen
237 variability considering contraction time, condition, and species as predictor variables. Finally, a
238 multivariate analysis of variance (MANOVA) was used to verify significant differences in iron
239 enrichment between species and condition groups and visualized with a Principal Component

240   Analysis (PCA). All statistical analyses were run in R v4.2.3 using *dplyr* (Wickham et al., 2023)
241   and *multcomp* packages (Hothorn, Bretz & Westfall, 2008) and visualized with the *ggplot2* package
242   (Wickham, 2016).
243
244   **Results**
245   The levels of dissolved iron measured in tanks ranged between 1.5 to 2.29 ± 0.12 µg L^{-1} (Table
246   1). *Cladocora caespitosa* exhibited a significant iron uptake with the highest uptake rate reaching
247   0.33 ± 0.16 µg cm^{-2} h^{-1} in the 50 nM Fe(III) treatment, and the lowest in the 100 nM Fe(III)
248   treatment (0.01 ± 0.03 µg cm^{-2} h^{-1}) (Kruskal-Wallis test, $X^2 = 9.154$, df = 3, $p < 0.05$; Table 1).
249   When comparing the individual conditions (Wilcoxon rank test) within *C. caespitosa* and *O.*
250   *patagonica* groups, no significant differences were detected.
251
252   *Coral metabolic rates.*
253   Iron uptake had divergent effects on the physiological characteristics of the two coral species
254   (Fig. 2). Specifically, in *C. caespitosa*, the respiration rate increased from 0.16 ± 0.02 µmol O_2
255   cm^{-2} h^{-1} in the 50 nM Fe(III) treatment to 0.29 ± 0.08 µmol O_2 cm^{-2} h^{-1} in the 100 nM Fe(III)
256   treatment (Kruskal-Wallis test, $X^2 = 11.6$, df = 3, $p < 0.01$). A similar pattern was observed in
257   photosynthetic rates, where net photosynthesis increased from 0.14 ± 0.02 µmol O_2 cm^{-2} h^{-1} in
258   the 20 nM Fe(III) to 0.29 ± 0.07 µmol O_2 cm^{-2} h^{-1} in 50 and 100 nM Fe(III) (Kruskal-Wallis test,
259    $X^2 = 12.2$, df = 3, $p < 0.01$), and gross photosynthesis increased from 0.3 ± 0.04 µmol O_2 cm^{-2} h^{-1}
260   in the 20 nM Fe(III) treatment to 0.64 ± 0.09 µmol O_2 cm^{-2} h^{-1} in the 50 nM Fe(III) and 100 nM
261   Fe(III) treatments (Kruskal-Wallis test, $X^2 = 11.8$, df = 3, $p < 0.01$). No detectable effect of iron
262   enrichment on the P:R ratio of *C. caespitosa*, but the maximum quantum yield of PSII (F_v/F_m)
263   increased slightly from 0.54 ± 0.03 in the 20 nM Fe(III) treatment to 0.63 ± 0.04 in the 100 nM
264   Fe(III) treatment (ANOVA, F = 3.83, $p < 0.05$, Table S1).
265   On the other hand, *O. patagonica* exhibited a decrease in respiration rates, continuously dropping
266   from 0.35 ± 0.09 at 20 nM Fe(III) to 0.18 ± 0.05 µmol O_2 cm^{-2} h^{-1} in the 100 nM Fe(III)
267   treatment (Kruskal-Wallis test, $X^2 = 19.1$, df = 3, $p < 0.01$). A similar pattern was observed in
268   photosynthetic rates, where net photosynthesis decreased at Fe(III) levels > 20 nM Fe(III) from
269   0.32 ± 0.06 to 0.20 ± 0.07 µmol O_2 cm^{-2} h^{-1} (Kruskal-Wallis test, $X^2 = 8.54$, df = 3, $p < 0.05$),
270   and gross photosynthesis continuously decreased at Fe(III) levels > 20 nM Fe(III), from $0.67 \pm$
271   0.14 to 0.37 ± 0.07 µmol O_2 cm^{-2} h^{-1} (Kruskal-Wallis test, $X^2 = 19.4$, df = 3, $p < 0.01$). A slight
272   increase was observed in the P:R ratio of *O. patagonica*, from 1.94 ± 0.16 in the 20 nM Fe(III)
273   treatment to 2.13 ± 0.18 and 2.21 ± 0.57 in the 50 nM and 100 nM Fe(III) treatments,
274   respectively (ANOVA, F = 8.29, $p < 0.01$). The F_v/F_m significantly decreased in *O. patagonica*
275   from 0.61 ± 0.18 in the Control condition to 0.28 ± 0.08 at > 20 nM Fe(III) (ANOVA, F = 10.94,
276    $p < 0.01$, Table S1).
277
278   *Variable chlorophyll fluorescence measurements.*

279   Differences in variable chlorophyll fluorescence parameters were evident between the two coral
280   species across iron enrichment levels, particularly in terms of the minimum and maximum
281   fluorescence yield, the PSII quantum yield, Y(II), and the derived relative electron transport rate,
282   rETR, during rapid light curve measurements (Fig. 3, Table S2). In *C. caespitosa*, the exposure
283   to 20 nM Fe(III) resulted in a significant enhancement of the minimum (Kruskal-Wallis test, X^2
284   = 92.187, df = 3), and maximum fluorescence yield (Kruskal-Wallis test, X^2 = 20.085, df = 3, p
285   < 0.01). The effective quantum yield, Y(II), remained unaffected, while the relative electron
286   transport rate, rETR, showed a decrease in the 100 nM Fe(III) treatment (Kruskal-Wallis test, X^2
287   = 9.225, df = 3, p < 0.05).
288   In *O. patagonica*, the exposure to 100 nM Fe(III) resulted in a significant enhancement of
289   minimum (Kruskal-Wallis test, X^2 = 110.06, df = 3) and maximum fluorescence yields
290   (Kruskal-Wallis test, X^2 = 17.625, df = 3, p < 0.01). A higher effective quantum yield, Y(II),
291   was observed at 20 nM and 50 nM Fe(III) treatment (Kruskal-Wallis test, X^2 = 15.109, df = 3, p
292   < 0.01), while no significant variations were observed in the relative electron transport rate..
293
294   *Spatial and temporal O_2 profiles.*
295   The O_2 availability within the gastric cavity of *C. caespitosa* and *O. patagonica* exhibited
296   significant differences across a depth range of 1-2 mm from the polyp's surface (Fig. 4A, Table
297   S3). Specifically, the availability of O_2 in *C. caespitosa* under dark conditions decreased when
298   transitioning from control conditions to iron enrichment conditions (Kruskal-Wallis test, X^2 =
299   115, df = 3, p < 0.01). Notably, the exposure to 50 nM and 100 nM Fe(III) resulted in hypoxic to
300   anoxic conditions (< 50 μmol O_2) in the dark. In the presence of 100 nM Fe(III), we also found a
301   marked reduction in O_2 availability when corals were exposed to light (Kruskal-Wallis test, X^2 =
302   32.9, df = 3, p < 0.01). A similar trend emerged in the gastric cavity of *O. patagonica* when
303   subjected to increasing Fe(III) levels, which led to diminished O_2 availability in comparison to
304   the control under both dark (Kruskal-Wallis test, X^2 = 163, df = 3, p < 0.01) and light (Kruskal-
305   Wallis test, X^2 = 11.1, df = 3, p < 0.05) conditions.
306   The O_2 levels measured overnight within the gastric cavity of *C. caespitosa* and *O. patagonica*
307   displayed significant variations based on different Fe levels (Fig. 4B). Specifically, when
308   transitioning from control conditions to Fe(III) enrichment conditions, the availability of O_2 in *C.*
309   *caespitosa* was significantly reduced from 125 ± 34.3 μmol O_2 L^{-1} under control conditions to
310   80.2 ± 43.2 μmol O_2 L^{-1} at 20 nM Fe(III), 48.3 ± 36.3 μmol O_2 L^{-1} at 50 nM Fe(III), and 23.8 ±
311   23.2 μmol O_2 L^{-1} at 100 nM Fe(III) (Kruskal-Wallis test, X^2 = 1475, df = 3, p < 0.01). Similarly,
312   in the case of *O. patagonica*, O_2 availability decreased in the presence of high Fe(III) levels,
313   from 219 ± 23 μmol O_2 L^{-1} in control conditions to 71.3 ± 32.8 μmol O_2 L^{-1} at 20 nM Fe(III),
314   52.3 ± 31.1 μmol O_2 L^{-1} at 50 nM Fe(III), and 11.7 ± 15 μmol O_2 L^{-1} at 100 nM Fe(III) (Kruskal-
315   Wallis test, X^2 = 2140, df = 3, p < 0.01).
316
317   *Coral tissue contraction.*

318   The O_2 levels within the gastric cavity of both *C. caespitosa* and *O. patagonica* corals exhibit a
319   significant correlation with the contraction time of the polyp ($p < 0.01$, Fig. 5, Table S4). The
320   linear regression model results indicated a significant association between contraction time,
321   Fe(III) exposure, and the O_2 level in the gastric cavity. Fe(III) enrichment had a notable effect on
322   contraction time, as reflected by its negative coefficient estimate of -29.80 ($p < 0.01$). This
323   negative coefficient suggests that, on average, when the corals are exposed to higher Fe(III)
324   levels, the tissue tends to contract more. Consequently, an increase in contraction time is
325   associated with a reduction in O_2 levels in both *C. caespitosa* and *O. patagonica* corals resulting
326   in a decrease of - 0.59 μmol O_2 L^{-1} and – 0.79 μmol O_2 L^{-1} per unit of contraction time,
327   respectively, as measured locally at the position of the microsensor tip in the gastric cavity.
328
329   *Multivariate analysis.*
330   The results of the multivariate analysis (MANOVA) indicated a significant impact of Fe(III)
331   exposure of corals on both conditions and species group ($p < 0.01$, Table S5). This influence was
332   also evident in the PCA plots representing the data distribution of variable chlorophyll
333   fluorescence and oxygen profile data (Fig. 6).
334

Discussion

336   While recent research has focused on the significance of iron as a limiting factor for
337   photosynthetic endosymbionts (Harland & Brown, 1989; Raven, Evans & Korb, 1999; Ferrier-
338   Pagès et al., 2001; Rädecker et al., 2017; Reich et al., 2020), knowledge of the physiological
339   consequences on the coral holobiont remains limited. This study is one of the first investigations
340   of the impact of Fe(III) enrichment on the photosynthesis and respiration of two Mediterranean
341   coral species, *Cladocora caespitosa* and *Oculina patagonica*. Overall, we found that high levels
342   (>50 nM) of Fe(III) are detrimental to the coral-Symbiodiniaceae symbiosis, decreasing the rates
343   of photosynthesis and increasing anoxia in the gastric cavity. Lower levels (< 50 nM) of Fe(III)
344   can have beneficial effects on photosynthetic efficiency, although it is species-dependent.
345   The susceptibility to Fe(III)-derived enhancement of coral photosynthetic activity is species-
346   specific. *C. caespitosa* corals inhabiting the Mediterranean Sea exhibit low frequency but high
347   magnitude of iron records in their skeleton (Royle et al., 2015) suggesting that this species is
348   naturally limited in iron but exposed to pulses of iron enrichment. Consequently, the exposure of
349   *C. caespitosa* to increased concentration of Fe(III) (up to 50 nM, in this study) resulted in
350   significant apparent uptake of Fe(III) (Table 1). This uptake was associated with elevated
351   respiratory and photosynthetic activities (Fig. 2), as well as an increase in minimum and
352   maximum fluorescence yield of photosystem II (Fig. 3). Therefore, the exposure to low levels of
353   Fe(III) might increase the photochemical quenching of iron-limited endosymbionts of *C.*
354   *caespitosa*, leading to increased quantum efficiency and fluorescence yield (Vassiliev' et al.;
355   Greene et al., 1992). However, the overall energetic productivity (P:R) remained largely
356   unchanged suggesting that the energy acquisition through photosynthesis was balanced by the
357   energy consumed through respiration.

358   In contrast, *O. patagonica* exhibited significantly lower respiration, photosynthesis, and
359   maximum PSII quantum yield (F_v/F_m) at all iron exposure levels, indicating a higher
360   susceptibility to reduced photosynthetic performance in response to increasing Fe(III) levels.
361   Nevertheless, increased maximum fluorescence and quantum yield of photosystem II were not
362   linked to increased photosynthetic activity, suggesting dynamic photoinhibition of the *O.*
363   *patagonica* endosymbionts under high levels of Fe(III) as a response to maintain the efficiency
364   of energy utilization through photosynthesis (Brown et al., 1999; Rodolfo-Metalpa et al., 2008).
365   This might indicate that *O. patagonica* is not iron-limited and increasing iron exposure may have
366   a detrimental effect on its photosynthetic performance. Moreover, elevated iron concentrations
367   might disrupt electron flow in the photosynthetic apparatus, as observed in the reduced rETR(II)
368   levels in *C. caespitosa*. We speculate that these variations might be attributed to the presence of
369   distinct Symbiodiniaceae hosted in *C. caespitosa* (*Symbiodinium microadriaticum*) and *O.*
370   *patagonica* (*Breviolum psygmophylum*) (Rodolfo-Metalpa et al., 2008; Casado-Amezúa et al.,
371   2014; Martinez et al., 2021; Davies et al., 2023). Different Symbiodiniaceae species may exhibit
372   differences in their tolerance to iron exposure, indicating species-specific nutrient requirements
373   (Reich et al., 2020; Camp et al., 2022). Species-specific responses to elevated Fe(III)
374   concentration also indicate that unique biogeochemical niches play a key role in the metabolic
375   compatibility of the coral-Symbiodiniaceae symbiosis (Grima et al. 2022). Distinct responses in
376   Fe(III) uptake observed in this study might be influenced by coral evolutionary origins, and
377   endosymbiont community structure, highlighting the importance of considering the relationship
378   between host and symbionts traits in nutrient cycling within the holobiont.
379   While these findings represent a first-time observation for Mediterranean corals, elevated iron
380   concentrations have been recognized to reduce photosynthetic capacity in tropical corals,
381   increasing their vulnerability to coral bleaching (Biscéré et al., 2018). Such reductions in
382   photosynthetic efficiency can have cascading effects on overall coral health, including growth,
383   reproduction, and resistance to environmental stressors (Ferrier-Pagès et al., 2001; Roth et al.,
384   2021). Elevated iron levels in seawater may thus also pose a potential stressor to Mediterranean
385   coral holobionts.
386   Our measurement of O_2 availability within the gastric cavity of *C. caespitosa* and *O. patagonica*
387   yielded the first insights into how respiratory activity within this compartment might be affected
388   by enhanced dissolved iron exposure. The O_2 level in the gastric cavity of both *C. caespitosa* and
389   *O. patagonica* in control conditions ranged from ~100 to 300 µmol O_2 L^{-1} (in dark and light,
390   respectively), in contrast to previous findings of hypoxia in the gastric cavity of the tropical coral
391   *Galaxea fascicularis* (Agostini et al., 2012), suggesting an enhanced capability of the
392   investigated Mediterranean corals to exchange O_2 with the surrounding seawater. However, this
393   difference might be due to the different polyp morphology, whose length and contraction rate
394   can affect the O2 availability within the gastric cavity. A decrease in O2 availability was
395   observed when transitioning from control to Fe(III) enrichment conditions (Fig. 4), where we
396   measured the development of hypoxic (< 50 µmol O_2 L^{-1}) to anoxic conditions in both corals
397   during daytime and overnight. These findings suggest that exposure to elevated Fe(III) reduces

398   O_2 levels within the gastric cavity of Mediterranean corals, which eventually may induce

399   hypoxia stress responses in the coral (Alderdice et al., 2021) and disrupt the delicate balance of

400   the coral microbiome (Bourne, Morrow & Webster, 2016; La Rivière, Garel & Bally, 2016). Fe(III)

401   uptake can be mediated by marine bacteria under both aerobic and anaerobic conditions (Weber,

402   Achenbach & Coates, 2006; Sandy & Butler, 2009). The increased availability of Fe(III) in

403   aerobic conditions might stimulate the reduction to ferrous iron, Fe(II), through bacterial

404   siderophore complexes (Sandy & Butler, 2009), to be used in the redox iron cycle. Fe(II) uptake,

405   on the other hand, is the predominant mechanism through ferrous iron uptake systems (i.e., ferric

406   uptake regulator) under anoxic conditions (Sandy & Butler, 2009).

407   Reduced O_2 levels in the gastric cavity might result from increased respiration of both host,

408   microbes, and endosymbionts (Zoccola et al., 2017), which could inhibit the energy metabolism

409   in coral symbiosis, reducing symbiont density and chlorophyll content, and inducing oxidative

410   stress (Turner et al., 2022; Zhang et al., 2023), with implications for energy allocation, growth,

411   and overall coral health (Agostini et al., 2012). Moreover, elevated Fe(III) concentration caused

412   increased contraction time in the pulsation rate of the coral polyps (Fig. 5), which in turn might

413   explain higher O_2 consumption within the coral gastric cavity via reduced O_2 exchange with

414   surrounding seawater. The pulsation rate of coral polyps might play a key role in their CO_2 / O_2

415   exchange and has been demonstrated to support the photosynthetic activity in zooxanthellate soft

416   corals (Kremien et al., 2013). A reduction in the pulsation rate has previously been linked to

417   pollution and eutrophication (Loya & Rinkevich, 1980; Ezzat et al., 2015; Thobor et al., 2022),

418   suggesting a behavioral response of the coral host to metal toxicity.

419   Our observations indicate that acute exposure to Fe(III) may result in species-specific responses

420   in corals. Our Fe exposure period was short as we wanted to mimic a pulse of dissolved Fe, in

421   line with observations in the skeleton of *C. caespitosa* (Royle et al., 2015). The short-term

422   exposure already had a beneficial effect on *C. caespitosa* and a negative effect on *O. patagonica*.

423   It would be interesting, in a future study, to assess whether these effects on Mediterranean corals

424   are confirmed with long-term exposure to low Fe concentrations. In addition, the Fe

425   concentrations used for the enrichments were theoretical concentrations and the actual

426   concentrations of bioavailable Fe(III) and its reduced form Fe(II) were most likely lower. The

427   levels of iron to which the corals were exposed can be considered 1 to 100 times higher than

428   typical concentrations found in coastal waters of the Mediterranean Sea, which typically receive

429   0.7-7 nM of dissolved iron and 0.8-14.5 nM of particulate iron (Sarthou & Jeandel, 2001).

430   However, high concentrations of Fe and other heavy metals have been measured in coastal

431   sediments of the Gulf of Genoa (Bertolotto et al. 2005) and the Adriatic Sea (Orlov et al. 2021),

432   where corals can thrive at high density. Resuspension of sediment can occur at regular times and

433   can release high levels of Fe into seawater. Therefore, the used iron concentrations in our study

434   simulated acute events that might result from sediment resuspension, exceptional runoff, or

435   increased nutrient loads. Thus, Mediterranean corals might already be exposed to enhanced

436   levels of dissolved iron and may not necessarily benefit from further iron enrichment. These

437   experimental limitations should be considered when interpreting the results and underscore the

438 need for further research with long-term exposure to comprehensively assess the effects of iron
439 on coral ecosystems.
440

Conclusions

442 Our study provides first insights into the intricate relationship between iron availability and coral
443 metabolism. The impact of iron on the coral holobiont is multifaceted and contingent upon
444 environmental factors, including ambient iron availability and the presence of other nutrients
445 (Harland & Brown, 1989; Rodriguez et al., 2016). Considering that iron seawater chemistry is
446 strongly influenced by environmental factors, such as ocean warming and acidification (Shi et
447 al., 2010, 2012), there is a pressing need to explore how these changes may alter iron availability
448 in the marine environment. Furthermore, the responses in different physiological parameters
449 observed in this study highlight the complex nature of host-symbiont and host-microbiome
450 interactions and their dependence on iron availability. Our findings emphasize the significance of
451 considering O_2 availability as a crucial factor when assessing the impact of iron enrichment on
452 coral health. Further research should focus on the exploration of the metabolic pathways affected
453 by altered O_2 levels, the bioavailability of iron in the redox cycle within the gastric cavity, and
454 the responses of photosynthetic endosymbionts as well as bacteria to iron enrichment. This will
455 refine our understanding of the broader consequences of iron enrichment and bioavailability in
456 coral reef ecosystems.
457

Acknowledgments

459 We thank Saul Ciriaco, Marco Segarich, and Verdiana Vellani from the Marine Protected Area
460 of Miramare, Trieste, and the University of Trieste (Italy) for their invaluable assistance in the
461 sampling of *Cladocora caespitosa* in Trieste and support in transporting the colonies to the CSM
462 laboratory. We thank Steen Færgemann Hansen from the Geoscience Department at the
463 University of Copenhagen (Denmark) for the ICP-MS analysis. We also thank Dr. Cesar O.
464 Pacherres from the Marine Biology Section, University of Copenhagen (Denmark) for the help in
465 the 3D printing of parts of respirometry chambers, Jonas Riff Larsen from the Niels Bohr
466 Institute, University of Copenhagen (Denmark) for the technical support with respirometry
467 chambers, and Elisenda Casabona Balcells for the illustrations of corals. Additionally, we
468 express our appreciation to laboratory technicians Cecile Rottier and Maria Isabelle Marcus for
469 their crucial contributions to the laboratory setup, and to Dr. Eric Beraud from the
470 Ecophysiology Laboratory at the Center Scientifique de Monaco for his assistance with PAM
471 measurements.

472

References

474 Agostini S, Suzuki Y, Higuchi T, Casareto BE, Yoshinaga K, Nakano Y, Fujimura H. 2012.
475   Biological and chemical characteristics of the coral gastric cavity. *Coral Reefs* 31:147–156.
476   DOI: 10.1007/S00338-011-0831-6.

477   Alderdice R, Suggett DJ, Cárdenas A, Hughes DJ, Kühl M, Pernice M, Voolstra CR. 2021.
478   Divergent expression of hypoxia response systems under deoxygenation in reef-forming
479   corals aligns with bleaching susceptibility. *Global Change Biology* 27:312–326. DOI:
480   10.1111/gcb.15436.
481   Baker NR, Oxborough K, Lawson T, Morison JIL. 2001. High resolution imaging of
482   photosynthetic activities of tissues, cells and chloroplasts in leaves. *Journal of Experimental*
483   *Botany* 52:615–621. DOI: 10.1093/JXB/52.356.615.
484   Beer S, Ilan M, Eshel A, Weil A, Brickner I. 1998. Use of pulse amplitude modulated (PAM)
485   fluorometry for in situ measurements of photosynthesis in two Red Sea faviid corals.
486   *Marine Biology* 131:607–612. DOI: 10.1007/s002270050352.
487   Behrenfeld MJ, Milligan AJ. 2013. Photophysiological Expressions of Iron Stress in
488   Phytoplankton. DOI: 10.1146/ANNUREV-MARINE-121211-172356.
489   Bertolotto RM, Tortarolo B, Frignani M, Bellucci LG, Albanese S, Cuneo C, Alvarado-Aguilar
490   D, Picca MR, Gollo E. 2005. Heavy metals in surficial coastal sediments of the Ligurian
491   Sea. *Marine Pollution Bulletin* 50 (3): 348-356. DOI: 10.1016/j.marpolbul.2004.12.002.
492   Bevilacqua S, Airoldi L, Ballesteros E, Benedetti-Cecchi L, Boero F, Bulleri F, Cebrian E,
493   Cerrano C, Claudet J, Colloca F, Coppari M, Di Franco A, Fraschetti S, Garrabou J,
494   Guarnieri G, Guerranti C, Guidetti P, Halpern BS, Katsanevakis S, Mangano MC, Micheli
495   F, Milazzo M, Pusceddu A, Renzi M, Rilov G, Sarà G, Terlizzi A. 2021. Mediterranean
496   rocky reefs in the Anthropocene: Present status and future concerns. *Advances in Marine*
497   *Biology* 89:1–51. DOI: 10.1016/BS.AMB.2021.08.001.
498   Biscéré T, Ferrier-Pagès C, Gilbert A, Pichler T, Houlbrèque F. 2018. Evidence for mitigation of
499   coral bleaching by manganese. *Scientific Reports 2018 8:1* 8:1–10. DOI: 10.1038/s41598-
500   018-34994-4.
501   Blain S, Tagliabue A. 2016. Iron Speciation in Seawater. *Iron Cycle in Oceans*:1–21. DOI:
502   10.1002/9781119136859.CH1.
503   Bonnet S, Guieu C. 2006. Atmospheric forcing on the annual iron cycle in the western
504   Mediterranean Sea: A 1-year survey. *Journal of Geophysical Research: Oceans* 111:9010.
505   DOI: 10.1029/2005JC003213.
506   Bourne DG, Morrow KM, Webster NS. 2016. Insights into the Coral Microbiome: Underpinning
507   the Health and Resilience of Reef Ecosystems. DOI: 10.1146/ANNUREV-MICRO-102215-
508   095440.
509   Brown BE, Ambarsari I, Warner ME, Fitt WK, Dunne RP, Gibb SW, Cummings DG. 1999.
510   Diurnal changes in photochemical efficiency and xanthophyll concentrations in shallow
511   water reef corals: Evidence for photoinhibition and photoprotection. *Coral Reefs* 18:99–
512   105. DOI: 10.1007/S003380050163/METRICS.
513   Camp EF, Nitschke MR, Clases D, Gonzalez de Vega R, Reich HG, Goyen S, Suggett DJ. 2022.
514   Micronutrient content drives elementome variability amongst the Symbiodiniaceae. *BMC*
515   *Plant Biology* 22:1–14. DOI: 10.1186/S12870-022-03512-0/TABLES/2.

516 Casado de Amezua P, Kersting D, Linares CL, Caroselli E, Garrabou J, Cerrano C, Ozalp B,
517   Terrón-Sigler A,, Betti F. 2015. *Cladocora caespitosa (Mediterranean Pillow Coral): The*
518   *IUCN Red List of Threatened Species 2015: e.T133142A75872554.*
519 Casado-Amezúa P, Machordom A, Bernardo J, González-Wangüemert M. 2014. New insights
520   into the genetic diversity of zooxanthellae in Mediterranean anthozoans. *Symbiosis* 63:41–
521   46. DOI: 10.1007/S13199-014-0286-Y/FIGURES/2.
522 D'Angelo C, Wiedenmann J. 2014. Impacts of nutrient enrichment on coral reefs: new
523   perspectives and implications for coastal management and reef survival. *Current Opinion in*
524   *Environmental Sustainability* 7:82–93. DOI: 10.1016/J.COSUST.2013.11.029.
525 Davies SW, Gamache MH, Howe-Kerr LI, Kriefall NG, Baker AC, Banaszak AT, Bay LK,
526   Bellantuono AJ, Bhattacharya D, Chan CX, Claar DC, Coffroth MA, Cunning R, Davy SK,
527   del Campo J, Díaz-Almeyda EM, Frommlet JC, Fuess LE, González-Pech RA, Goulet TL,
528   Hoadley KD, Howells EJ, Hume BCC, Kemp DW, Kenkel CD, Kitchen SA, LaJeunesse
529   TC, Lin S, McIlroy SE, McMinds R, Nitschke MR, Oakley CA, Peixoto RS, Prada C,
530   Putnam HM, Quigley K, Reich HG, Reimer JD, Rodriguez-Lanetty M, Rosales SM, Saad
531   OS, Sampayo EM, Santos SR, Shoguchi E, Smith EG, Stat M, Stephens TG, Strader ME,
532   Suggett DJ, Swain TD, Tran C, Traylor-Knowles N, Voolstra CR, Warner ME, Weis VM,
533   Wright RM, Xiang T, Yamashita H, Ziegler M, Correa AMS, Parkinson JE. 2023. Building
534   consensus around the assessment and interpretation of Symbiodiniaceae diversity. *PeerJ*
535   11:e15023. DOI: 10.7717/PEERJ.15023.
536 Entsch B, Sim RG, Hatcher BG. 1983. Indications from photosynthetic components that iron is a
537   limiting nutrient in primary producers on coral reefs. *Marine Biology* 73:17–30. DOI:
538   10.1007/BF00396281.
539 Ezzat L, Maguer JF, Grover R, Ferrier-Pagés C. 2015. New insights into carbon acquisition and
540   exchanges within the coral–dinoflagellate symbiosis under NH_4^+ and NO_3^- supply.
541   *Proceedings of the Royal Society B: Biological Sciences* 282. DOI:
542   10.1098/RSPB.2015.0610.
543 Ferrier-Pagès C, Schoelzke V, Jaubert J, Muscatine L, Hoegh-Guldberg O. 2001. Response of a
544   scleractinian coral, Stylophora pistillata, to iron and nitrate enrichment. *Journal of*
545   *Experimental Marine Biology and Ecology* 259:249–261. DOI: 10.1016/S0022-
546   0981(01)00241-6.
547 Fine M, Zibrowius H, Loya Y. 2001. Oculina patagonica: A non-lessepsian scleractinian coral
548   invading the Mediterranean sea. *Marine Biology* 138:1195–1203. DOI:
549   10.1007/S002270100539/METRICS.
550 Gallisai R, Peters F, Volpe G, Basart S, Baldasano JM. 2014. Saharan Dust Deposition May
551   Affect Phytoplankton Growth in the Mediterranean Sea at Ecological Time Scales. *PLOS*
552   *ONE* 9:e110762. DOI: 10.1371/JOURNAL.PONE.0110762.
553 GEOTRACES Intermediate Data Product Group (2021). The GEOTRACES Intermediate Data
554   Product 2021 (IDP2021). NERC EDS British Oceanographic Data Centre NOC.
555   doi:10.5285/cf2d9ba9-d51d-3b7c-e053-8486abc0f5fd.Genty B, Briantais JM, Baker NR.

556   1989. The relationship between the quantum yield of photosynthetic electron transport and
557   quenching of chlorophyll fluorescence. *Biochimica et Biophysica Acta (BBA) - General*
558   *Subjects* 990:87–92. DOI: 10.1016/S0304-4165(89)80016-9.

559   Gledhill M, McCormack P, Ussher S, Achterberg EP, Mantoura RFC, Worsfold PJ. 2004.
560   Production of siderophore type chelates by mixed bacterioplankton populations in nutrient
561   enriched seawater incubations. *Marine Chemistry* 88:75–83. DOI:
562   10.1016/J.MARCHEM.2004.03.003.

563   Greene RM, Geider RJ, Kolber Z, Falkowski PG. 1992. Iron-induced Changes in Light
564   Harvesting and Photochemical Energy Conversion Processes in Eukaryotic Marine Algae'.
565   *Plant Physiol* 100:565–575.

566   Grima AJ, Clases D, Gonzalez de Vega R, Nitschke MR, Goyen S, Suggett DJ, Camp EF. 2022.
567   Species-specific elementomes for scleractinian coral hosts and their associated
568   Symbiodiniaceae. *Coral Reefs* 41, 1115–1130 (2022). https://doi.org/10.1007/s00338-022-
569   02259-2

570   Guerzoni S, Chester R, Dulac F, Herut B, Loÿe-Pilot MD, Measures C, Migon C, Molinaroli E,
571   Moulin C, Rossini P, Saydam C, Soudine A, Ziveri P. 1999. The role of atmospheric
572   deposition in the biogeochemistry of the Mediterranean Sea. *Progress in Oceanography*
573   44:147–190. DOI: 10.1016/S0079-6611(99)00024-5.

574   Harland AD, Brown BE. 1989. Metal tolerance in the scleractinian coral *Porites lutea*. *Marine*
575   *Pollution Bulletin* 20:353–357. DOI: 10.1016/0025-326X(89)90159-8.

576   Haro S, Brodersen KE, Bohórquez J, Papspyrou S, Corzo A, Kühl M. 2019. Radiative energy
577   budget in a microbial mat under different irradiance and tidal conditions. *Microbial Ecology*
578   77:852-865.

579   Hassler CS, Schoemann V, Nichols CM, Butler ECV, Boyd PW. 2011. Saccharides enhance iron
580   bioavailability to southern ocean phytoplankton. *Proceedings of the National Academy of*
581   *Sciences of the United States of America* 108:1076–1081. DOI:
582   10.1073/PNAS.1010963108.

583   Hoeksema BW. 2017. The hidden biodiversity of tropical coral reefs. *Biodiversity* 18:8–12. DOI:
584   10.1080/14888386.2017.1307787.

585   Hothorn T, Bretz F, Westfall P. 2008. Simultaneous Inference in General Parametric Models.
586   *Biometrical Journal* 50:346–363. DOI: 10.1002/BIMJ.200810425.

587   Houk P, Comeros-Raynal M, Lawrence A, Sudek M, Vaeoso M, McGuire K, Regis J. 2020.
588   Nutrient thresholds to protect water quality and coral reefs. *Marine Pollution Bulletin*
589   159:111451. DOI: 10.1016/j.marpolbul.2020.111451.

590   Houlbrèque F, Ferrier-Pagès C. 2009. Heterotrophy in Tropical Scleractinian Corals. *Biological*
591   *Reviews* 84:1–17. DOI: 10.1111/J.1469-185X.2008.00058.X.

592   Hughes DJ, Raina JB, Nielsen DA, Suggett DJ, Kühl M. 2022. Disentangling compartment
593   functions in sessile marine invertebrates. *Trends in Ecology and Evolution* 37:740–748.
594   DOI: 10.1016/j.tree.2022.04.008.

595   Ingrosso G, Abbiati M, Badalamenti F, Bavestrello G, Belmonte G, Cannas R, Benedetti-Cecchi
596   L, Bertolino M, Bevilacqua S, Bianchi CN, Bo M, Boscari E, Cardone F, Cattaneo-Vietti R,
597   Cau A, Cerrano C, Chemello R, Chimienti G, Congiu L, Corriero G, Costantini F, De Leo
598   F, Donnarumma L, Falace A, Fraschetti S, Giangrande A, Gravina MF, Guarnieri G,
599   Mastrototaro F, Milazzo M, Morri C, Musco L, Pezzolesi L, Piraino S, Prada F, Ponti M,
600   Rindi F, Russo GF, Sandulli R, Villamor A, Zane L, Boero F. 2018. Mediterranean
601   Bioconstructions Along the Italian Coast. *Advances in Marine Biology* 79:61–136. DOI:
602   10.1016/BS.AMB.2018.05.001.
603   Johnson KS, Gordon RM, Coale KH. 1997. What controls dissolved iron concentrations in the
604   world ocean? *Marine Chemistry* 57:137–161.
605   Kremien M, Shavit U, Mass T, Genin A. 2013. Benefit of pulsation in soft corals. *Proceedings of
606   the National Academy of Sciences of the United States of America* 110:8978–8983. DOI:
607   10.1073/PNAS.1301826110.
608   Krishnamurthy A, Moore JK, Mahowald N, Luo C, Zender CS. 2010. Impacts of atmospheric
609   nutrient inputs on marine biogeochemistry. *Journal of Geophysical Research:
610   Biogeosciences* 115:1006. DOI: 10.1029/2009JG001115.
611   Kružić P, Benković L. 2008. Bioconstructional features of the coral *Cladocora caespitosa*
612   (Anthozoa, Scleractinia) in the Adriatic Sea (Croatia). *Marine Ecology* 29:125–139. DOI:
613   10.1111/J.1439-0485.2008.00220.X.
614   Leigh-Smith J, Reichelt-Brushett A, Rose AL. 2018. The characterization of iron (III) in
615   seawater and related toxicity to early life stages of scleractinian corals. *Environmental
616   Toxicology and Chemistry* 37:1104–1114. DOI: 10.1002/ETC.4043.
617   Liu X, Millero FJ. 2002. The solubility of iron in seawater. *Marine Chemistry* 77:43–54. DOI:
618   10.1016/S0304-4203(01)00074-3.
619   Loya Y, Rinkevich B. 1980. Effects of Oil Pollution on Coral Reef Communities. *Marine
620   Ecology Progress Series* 3:167–180.
621   Mahowald NM, Baker AR, Bergametti G, Brooks N, Duce RA, Jickells TD, Kubilay N,
622   Prospero JM, Tegen I. 2005. Atmospheric global dust cycle and iron inputs to the ocean.
623   *Global Biogeochemical Cycles* 19. DOI: 10.1029/2004GB002402.
624   Marsh JA. 1970. Primary Productivity of Reef-Building Calcareous Red Algae. *Ecology* 51:255–
625   263. DOI: 10.2307/1933661.
626   Martinez S, Bellworthy J, Ferrier-Pagès C, Mass T. 2021. Selection of mesophotic habitats by
627   *Oculina patagonica* in the Eastern Mediterranean Sea following global warming. *Scientific
628   Reports 2021 11:1* 11:1–15. DOI: 10.1038/s41598-021-97447-5.
629   Molari M, Guilini K, Lott C, Weber M, De Beer D, Meyer S, Ramette A, Wegener G,
630   Wenzhöfer F, Martin D, Cibic T, De Vittor C, Vanreusel A, Boetius A. 2018. CO2 leakage
631   alters biogeochemical and ecological functions of submarine sands. *Science Advances* 4.
632   DOI: 10.1126/SCIADV.AAO2040.
633   Morrissey J, Sutak R, Paz-Yepes J, Tanaka A, Moustafa A, Veluchamy A, Thomas Y, Botebol
634   H, Bouget FY, McQuaid JB, Tirichine L, Allen AE, Lesuisse E, Bowler C. 2015. A Novel

635   Protein, Ubiquitous in Marine Phytoplankton, Concentrates Iron at the Cell Surface and
636   Facilitates Uptake. *Current Biology* 25:364–371. DOI: 10.1016/J.CUB.2014.12.004.

637 Muscatine L, Porter JW. 1977. Reef Corals: Mutualistic Symbioses Adapted to Nutrient-Poor
638   Environments. *BioScience* 27:454–460. DOI: 10.2307/1297526.

639 Orlov M, Kramarić R, Romac I, Maričević N 2022. Heavy Metals in the Sediment of the Islands
640   of Lastovo and Mljet and the City of Dubrovnik. *NAŠE MORE*: znanstveni časopis za more
641   i pomorstvo, 69(1), 16-21. DOI 10.17818/NM/2022/1.3.

642 Peirano A, Morri C, Bianchi CN, Aguirre J, Antonioli F, Calzetta G, Carobene L, Mastronuzzi
643   G, Orrù P. 2004. The Mediterranean coral *Cladocora caespitosa*: A proxy for past climate
644   fluctuations? *Global and Planetary Change* 40:195–200. DOI: 10.1016/S0921-
645   8181(03)00110-3.

646 Ponti M, Linares C, Cerrano C, Rodolfo-Metalpa R, Hoeksema BW. 2021. Editorial: Biogenic
647   Reefs at Risk: Facing Globally Widespread Local Threats and Their Interaction With
648   Climate Change. *Frontiers in Marine Science* 8:1688. DOI: 10.3389/FMARS.2021.793038.

649 Rädecker N, Pogoreutz C, Ziegler M, Ashok A, Barreto MM, Chaidez V, Grupstra CGB, Ng
650   YM, Perna G, Aranda M, Voolstra CR. 2017. Assessing the effects of iron enrichment
651   across holobiont compartments reveals reduced microbial nitrogen fixation in the Red Sea
652   coral Pocillopora verrucosa. *Ecology and Evolution* 7:6614–6621. DOI:
653   10.1002/ECE3.3293.

654 Ralph PJ, Gademann R. 2005. Rapid light curves: A powerful tool to assess photosynthetic
655   activity. *Aquatic Botany* 82:222–237. DOI: 10.1016/J.AQUABOT.2005.02.006.

656 Ralph P, Gademann R, Larkum A, Schreiber U. 1999. In situ underwater measurements of
657   photosynthetic activity of coral zooxanthellae and other reef-dwelling dinoflagellate
658   endosymbionts. *Marine Ecology Progress Series* 180:139–147. DOI: 10.3354/meps180139.

659 Raven JA, Evans MCW, Korb RE. 1999. The role of trace metals in photosynthetic electron
660   transport in O2-evolving organisms. *Photosynthesis Research* 60:111–150. DOI:
661   10.1023/A:1006282714942.

662 Reich HG, Camp EF, Roger LM, Putnam HM. 2023. The trace metal economy of the coral
663   holobiont: supplies, demands and exchanges. *Biological Reviews* 98:623–642. DOI:
664   10.1111/brv.12922.

665 Reich HG, Rodriguez IB, LaJeunesse TC, Ho TY. 2020. Endosymbiotic dinoflagellates pump
666   iron: differences in iron and other trace metal needs among the Symbiodiniaceae. *Coral
667   Reefs* 39:915–927. DOI: 10.1007/s00338-020-01911-z.

668 Reichelt-Brushett AJ, McOrist G. 2003. Trace metals in the living and nonliving components of
669   scleractinian corals. *Marine Pollution Bulletin* 46:1573–1582. DOI: 10.1016/S0025-
670   326X(03)00323-0.

671 La Rivière M, Garel M, Bally M. 2016. Localization of endobacteria in the gastrodermis of a
672   Mediterranean gorgonian coral, *Paramuricea clavata*, using fluorescence in situ
673   hybridization. *Marine Biology* 163:1–9. DOI: 10.1007/S00227-016-2975-Y.

Rodolfo-Metalpa R, Reynaud S, Allemand D, Ferrier-Pagès C. 2008. Temporal and depth responses of two temperate corals, *Cladocora caespitosa* and *Oculina patagonica*, from the North Mediterranean Sea. *Marine Ecology Progress Series* 369:103–114. DOI: 10.3354/MEPS07608.

Rodolfo-Metalpa R, Richard C, Allemand D, Bianchi CN, Morri C, Ferrier-Pagès C. 2006. Response of zooxanthellae in symbiosis with the Mediterranean corals *Cladocora caespitosa* and *Oculina patagonica* to elevated temperatures. *Marine Biology* 150:45–55. DOI: 10.1007/S00227-006-0329-X.

Rodriguez IB, Lin S, Ho J, Ho TY. 2016. Effects of trace metal concentrations on the growth of the coral endosymbiont Symbiodinium kawagutii. *Frontiers in Microbiology* 7:154024. DOI: 10.3389/FMICB.2016.0008.

Roth F, RAdecker N, Carvalho S, Duarte CM, Saderne V, Anton A, Silva L, Calleja ML, MorÁn XAG, Voolstra CR, Kürten B, Jones BH, Wild C. 2021. High summer temperatures amplify functional differences between coral- and algae-dominated reef communities. *Ecology* 102:e03226. DOI: 10.1002/ecy.3226.

Royle SH, Andrews JE, Turner J, Kružić P. 2015. Environmental and diagenetic records from trace elements in the Mediterranean coral *Cladocora caespitosa*. *Palaeogeography, Palaeoclimatology, Palaeoecology* 440:734–749. DOI: 10.1016/J.PALAEO.2015.10.010.

Sandy M, Butler A. 2009. Microbial Iron Acquisition: Marine and Terrestrial Siderophores. *Chemical reviews* 109:4580. DOI: 10.1021/CR9002787.

Sarthou G, Jeandel C. 2001a. Seasonal variations of iron concentrations in the Ligurian Sea and iron budget in the Western Mediterranean Sea. *Marine Chemistry* 74:115–129. DOI: 10.1016/S0304-4203(00)00119-5.

Sarthou G, Jeandel C. 2001b. Seasonal variations of iron concentrations in the Ligurian Sea and iron budget in the Western Mediterranean Sea. *Marine Chemistry* 74:115–129. DOI: 10.1016/S0304-4203(00)00119-5.

Schneider CA, Rasband WS, Eliceiri KW. 2012. NIH Image to ImageJ: 25 years of image analysis. *Nature Methods 2012 9:7* 9:671–675. DOI: 10.1038/nmeth.2089.

Schreiber U. 2004. Pulse-Amplitude-Modulation (PAM) Fluorometry and Saturation Pulse Method: An Overview. *Chlorophyll a Fluorescence*:279–319. DOI: 10.1007/978-1-4020-3218-9_11.

Serôdio J, Da Silva JM, Catarino F. 1997. Nondestructive tracing of migratory rhythms of intertidal benthic microalgae using in vivo chlorophyll a fluorescence. *Journal of Phycology* 33:542–553. DOI: 10.1111/J.0022-3646.1997.00542.X.

Shi D, Kranz SA, Kim JM, Morel FMM. 2012. Ocean acidification slows nitrogen fixation and growth in the dominant diazotroph Trichodesmium under low-iron conditions. *Proceedings of the National Academy of Sciences of the United States of America* 109:E3094. DOI: 10.1073/PNAS.1216012109.

712 Shi D, Xu Y, Hopkinson BM, Morel FMM. 2010. Effect of ocean acidification on iron
713   availability to marine phytoplankton. *Science* 327:676–679. DOI:
714   10.1126/SCIENCE.1183517.

715 Shick JM, Iglic K, Wells ML, Trick CG, Doyle J, Dunlap WC. 2011. Responses to iron
716   limitation in two colonies of Stylophora pistillata exposed to high temperature: Implications
717   for coral bleaching. *Limnology and Oceanography* 56:813–828. DOI:
718   10.4319/LO.2011.56.3.0813.

719 Sutak R, Camadro JM, Lesuisse E. 2020. Iron Uptake Mechanisms in Marine Phytoplankton.
720   *Frontiers in Microbiology* 11:566691. DOI: 10.3389/FMICB.2020.566691.

721 Thobor B, Tilstra A, Bourne DG, Springer K, Mezger SD, Struck U, Bockelmann F,
722   Zimmermann L, Yánez Suárez AB, Klinke A, Wild C. 2022. The pulsating soft coral *Xenia*
723   *umbellata* shows high resistance to warming when nitrate concentrations are low. *Scientific*
724   *Reports 2022 12:1* 12:1–17. DOI: 10.1038/s41598-022-21110-w.

725 Trampe E, Kolbowski J, Schreiber U, Kühl M. 2011. Rapid assessment of different oxygenic
726   phototrophs and single-cell photosynthesis with multicolour variable chlorophyll
727   fluorescence imaging. *Marine Biology* 158:1667–1675. DOI: 10.1007/S00227-011-1663-1.

728 Turner JR, Carlos Hernández J, Deleja M, Paula JR, Repolho T, Franzitta M, Baptista M, Lopes
729   V, Simão S, Fonseca VF, Duarte B, Rosa R. 2022. Effects of Hypoxia on Coral
730   Photobiology and Oxidative Stress. *Biology* 2022:1068. DOI: 10.3390/biology11071068.

731 Vassiliev' LR, Kolber Z, Wyman KD, Mauzerall D, Shukla VK, Falkowski PC. Effects of lron
732   Limitation on Photosystem II Composition and Light Utilization in Dunaliella teutiolecta'.
733   *Plant Physiol* 1:963–972.

734 Wagener T, Guieu C, Leblond N. 2010. Effects of dust deposition on iron cycle in the surface
735   Mediterranean Sea: Results from a mesocosm seeding experiment. *Biogeosciences* 7:3769–
736   3781. DOI: 10.5194/BG-7-3769-2010.

737 Walte TD, Morel FMM. 1984. Photoreductive dissolution of colloidal iron oxides in natural
738   waters. *Environmental science & technology* 18:860–868. DOI: 10.1021/ES00129A010.

739 Weber KA, Achenbach LA, Coates JD. 2006. Microorganisms pumping iron: anaerobic
740   microbial iron oxidation and reduction. *Nature Reviews Microbiology 2006 4:10* 4:752–
741   764. DOI: 10.1038/nrmicro1490.

742 Wickham H. 2016. ggplot2: Elegant graphics for data analysis. Springer-Verlag New York.
743   ISBN 978-3-319-24277-4, https://ggplot2.tidyverse.org.

744 Wickham H, François R, Henry L, Müller K, Vaughan D. 2023. dplyr: A grammar of data
745   manipulation. R package version 1.1.4, https://github.com/tidyverse/dplyr,
746   https://dplyr.tidyverse.org.

747 Zhang K, Wu Z, Liu Z, Tang J, Cai W, An M, Zhou Z. 2023. Acute hypoxia induces reduction of
748   algal symbiont density and suppression of energy metabolism in the scleractinian coral
749   *Pocillopora damicornis*. *Marine Pollution Bulletin* 191:114897. DOI:
750   10.1016/J.MARPOLBUL.2023.114897.

751 Zoccola D, Morain J, Pagès G, Caminiti-Segonds N, Giuliano S, Tambutté S, Allemand D. 2017.
752   Structural and functional analysis of coral Hypoxia Inducible Factor. *PLOS ONE*
753   12:e0186262. DOI: 10.1371/JOURNAL.PONE.0186262.
754

Experimental conditions and Fe uptake in *C. caespitosa* and *O. patagonica*.

Condition indicates the pulses of Fe(III) added to expose corals to 0, 20, 50, and 100 nM Fe/day. Fe(III) uptake is calculated as the difference between Fe concentrations in the seawater and in the chambers at the end of incubation. Kruskal-Wallis test, Chi-squared = test statistic H; Df = degrees of freedom. Values are average and standard deviation.

Species	Condition	Fe(III) seawater $\mu g\,L^{-1}$	Fe(III) uptake $\mu g\,cm^{-2}\,h^{-1}$	Chi-squared	Df	p-value
C. caespitosa	Control	1.67 ± 0.12	0.01 ± 0.07	9.154	3	< 0.05
	20 nM	1.77 ± 0.15	0.20 ± 0.15			
	50 nM	1.50 ± 1.53	0.33 ± 0.16			
	100 nM	2.29 ± 0.12	0.01 ± 0.03			
O. patagonica	Control	1.67 ± 0.12	0.00 ± 0.03	4.378	3	*n.s.*
	20 nM	1.77 ± 0.15	0.09 ± 0.14			
	50 nM	1.50 ± 1.53	0.07 ± 0.33			
	100 nM	2.29 ± 0.12	0.00 ± 0.04			

Figure 1

Schematic representation of internal coral polyps' features.

(A) *Cladocora caespitosa*, and (B) *Oculina patagonica:* polyps size, gastric cavity, and skeleton. Digital illustrations are openly available in Zenodo at https://doi.org/10.5281/zenodo.10781253.
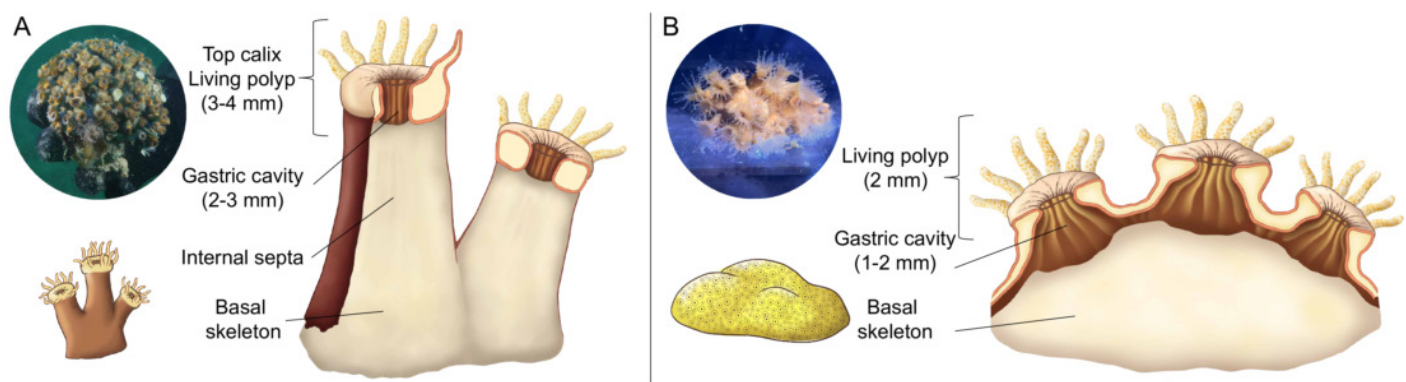
Figure 2

Physiological parameters of corals under increasing Fe(III) exposure.

(A) Respiration rate, (B) net photosynthesis rate, (C) gross photosynthesis rate, (D) ratio of gross photosynthesis to respiration (P:R), and (E) maximum quantum efficiency of Photosystem II (F_v/F_m) in *C. caespitosa* and *O. patagonica*. Condition indicates the pulses of Fe(III) added to expose corals to 0, 20, 50, and 100 nM Fe/day. The letters above the bars indicate significant differences among conditions ($p < 0.05$).
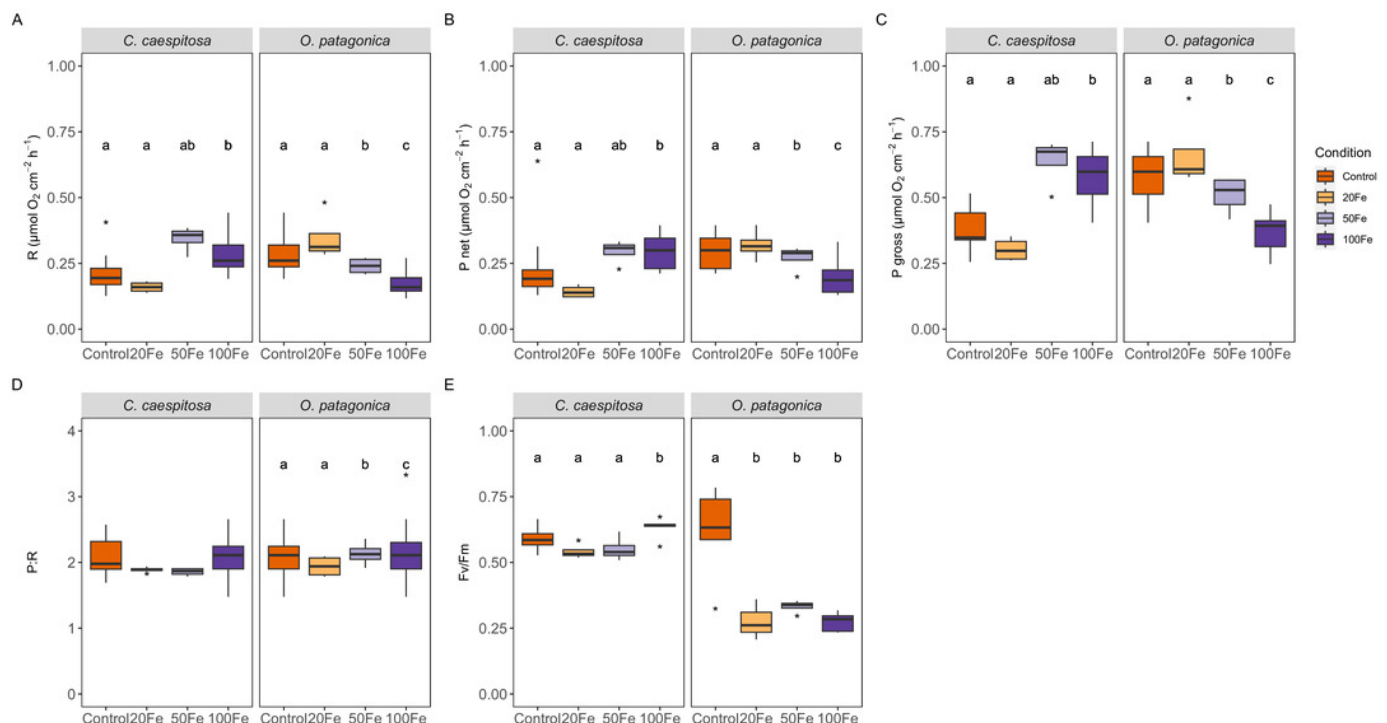
Figure 3

Variable chlorophyll fluorescence measurements

(A) Minimum fluorescence yield; (B) maximum fluorescence yield; (C) effective PSII quantum yield, YII, and (D) derived relative electron transport rates, rETR, as a function of rapidly increasing photon irradiance, i.e., RLC measurements. Condition indicates the pulses of Fe(III) added to expose corals to 0, 20, 50, and 100 nM Fe/day. The continuous line indicates the mean values.
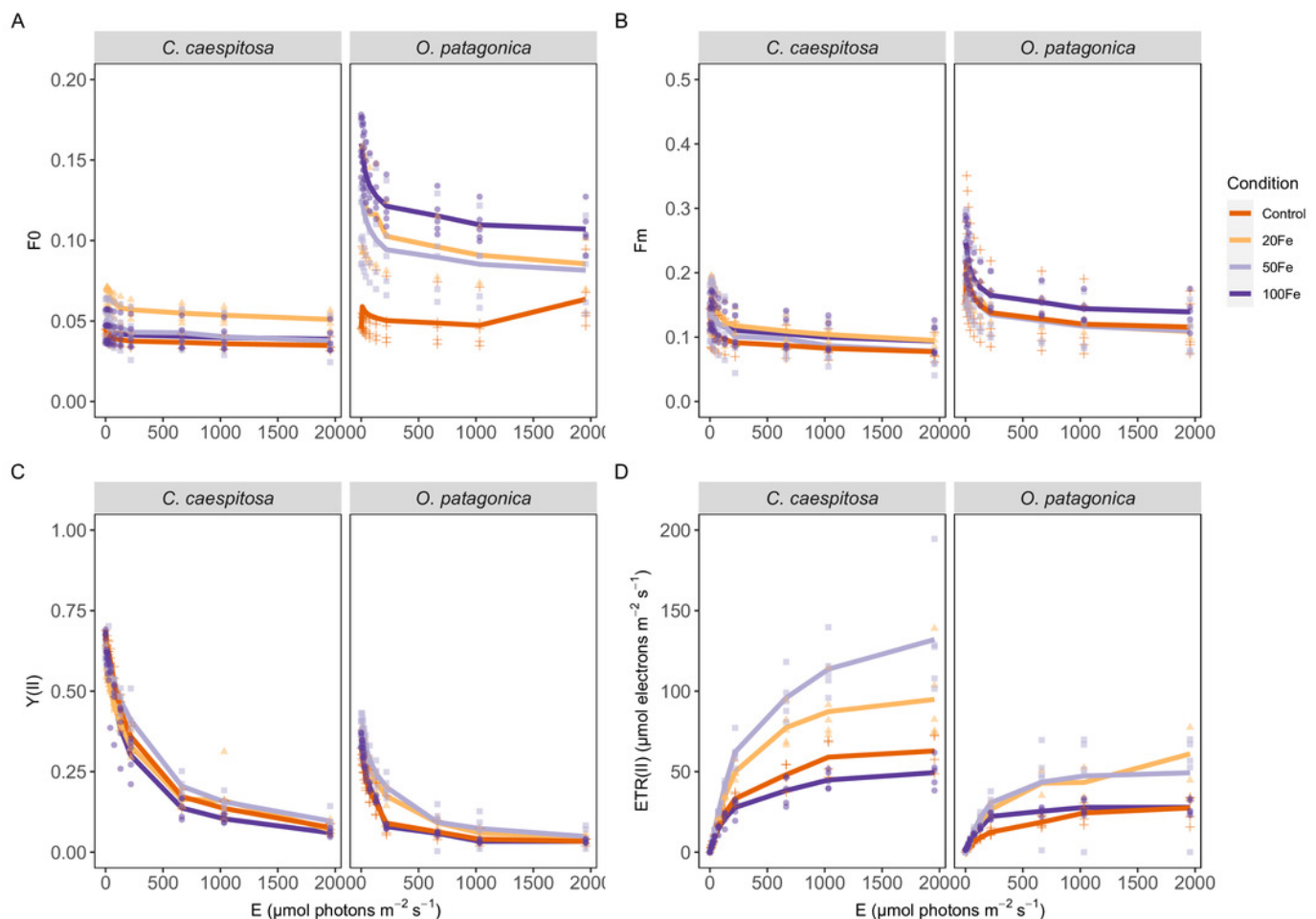
Figure 4

Oxygen distribution and dynamics in the gastric cavity of coral specimens.

(A) Depth profiles of O_2 concentration in the gastric cavity of *C. caespitosa* and *O. patagonica* measured under dark and light conditions; (B) temporal variation in O_2 concentration measured in *C. caespitosa* and *O. patagonica* under dark condition in the bottom of the gastric cavity overnight. Condition indicates the pulses of Fe(III) added to expose corals to 0, 20, 50, and 100 nM Fe/day. The dotted line indicates the polyp surface level. The continuous line indicates the trend line using *loess* method, with the shaded area as confidence intervals (95%).
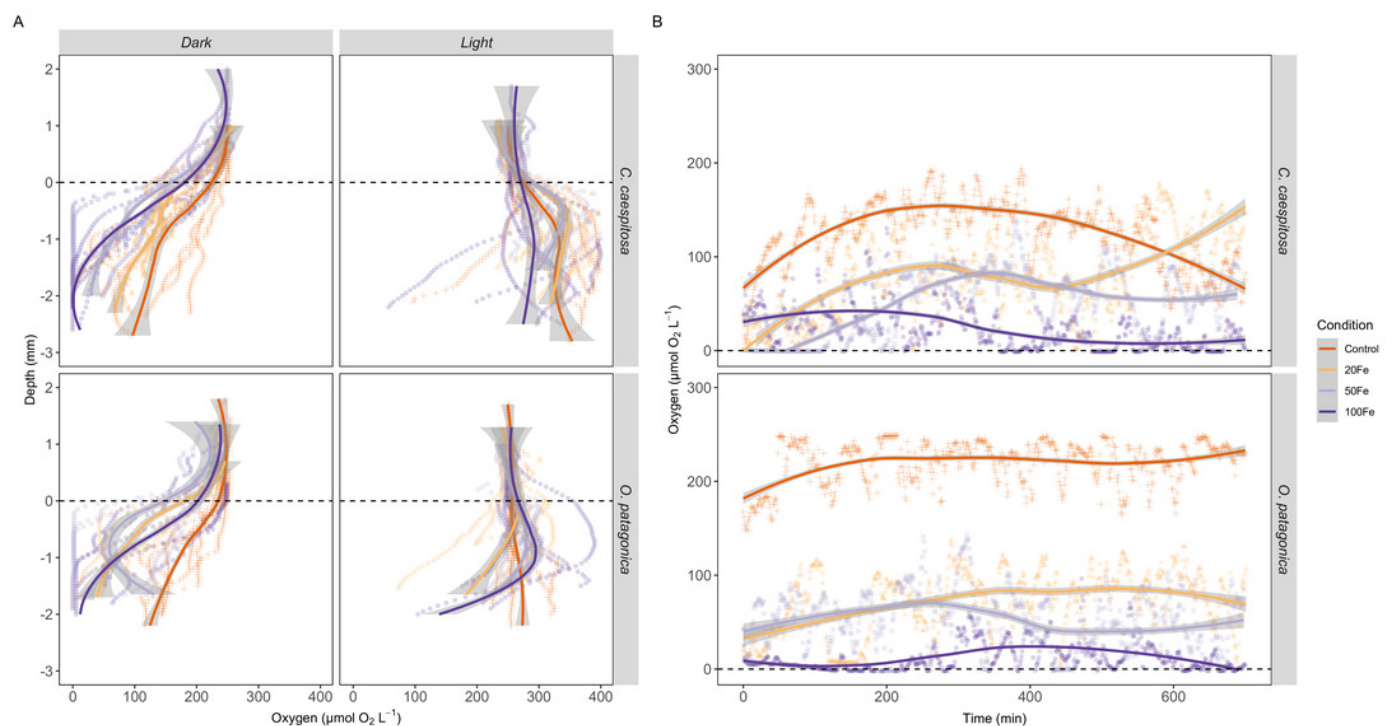
Figure 5

The relationship between O_2 concentration and polyp contraction time (%) in the gastric cavity of coral specimens.

O_2 concentration in the gastric cavity of *C. caespitosa* and *O. patagonica* measured under dark condition relative to contraction time of the polyp. The dotted line indicates the hypoxia level at 50 µmol O_2 L^{-1} (equivalent to 2 mg O_2 L^{-1}). The red continuous line indicates a linear regression model ($R^2 = 0.40$, F = 1046, Df = 6257, p < 0.01).

O. patagonica / C. caespitosa panels: Oxygen (µmol O_2 L^{-1}) vs Contraction Time (%)

$R^2 = 0.04$ (C. caespitosa)
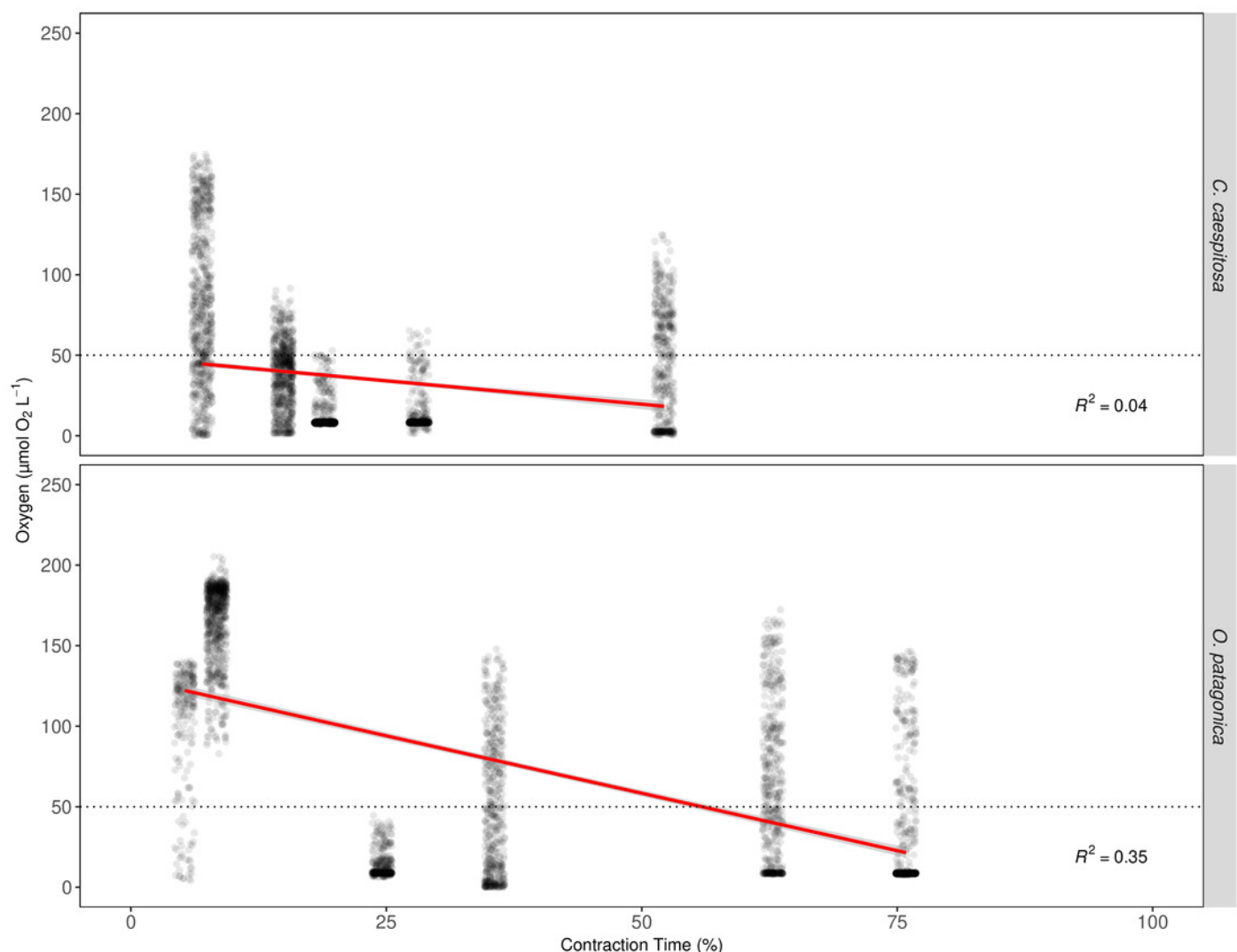
$R^2 = 0.35$ (O. patagonica)

Figure 6

Principal Component Analysis (PCA) plots.

(A) Chlorophyll fluorescence parameters; and (B) O_2 concentration in the gastric cavity of *C. caespitosa* and *O. patagonica*. Condition indicates the pulses of Fe(III) added to expose corals to 0, 20, 50, and 100 nM Fe/day.